Bioprocess-Inspired Synthesis

Deutsche Ausgabe: DOI: 10.1002/ange.201509906
Internationale Ausgabe: DOI: 10.1002/anie.201509906

Mussel-Directed Synthesis of Nitrogen-Doped Anatase TiO_2

*Jingjing Xie, Hao Xie, Bao-Lian Su, Yi-bing Cheng, Xiaodong Du, Hui Zeng, Menghu Wang, Weimin Wang, Hao Wang, and Zhengyi Fu**

Abstract: *Structure-forming processes leading to biominerals are well worth learning in pursuit of new synthetic techniques. Strategies that attempt to mimic nature in vitro cannot replace an entire complex natural organism, requiring ingenuity beyond chemists' hands. A "bioprocess-inspired synthesis" is demonstrated for fabrication of N-doped TiO_2 materials at ambient temperature by direct implantation of precursor into living mussels. The amorphous precursor transforms into N-doped anatase TiO_2 with a hierarchical nanostructure. Synthetic TiO_2 exhibits high phase stability and enhanced visible-light photocatalytic activity as a result of modifications to its band gap during in vivo mineralization. Intracellular proteins were found to be involved in TiO_2 mineralization. Our findings may inspire material production by new synthetic techniques, especially under environmentally benign conditions.*

In studying and mimicking the well-defined structures or unique functions of biomaterials,[1–3] scientists have succeeded in designing and synthesizing bio-inspired materials or bio-inspired functions.[4–6] Furthermore, in contrast with anthropogenic technologies that commonly require harsh conditions, the fantastic structure-forming processes found in biological systems are the results of many billions of years of evolution, leading to efficient and accurate fabrication of biominerals under environmentally benign conditions.[7,8] Hence, natural structure-forming processes themselves are also worth understanding when developing new synthesis techniques for materials. This field of research is referred to as "bioprocess-inspired fabrication". To date, bioprocess-inspired work focuses on using organic matrices, including proteins, as templates for directing the formation of inorganic materials in vitro.[9–11] However, in most situations, a single protein or a combination of several proteins cannot be substituted for an entire natural organism, which is a capable cradle for the growth of biominerals (formation of a pearl inside a mussel for example). The complexity and ingenuity of biological systems are still beyond the skills of chemists to recreate.[12,13] Herein, we propose a strategy that capitalizes on natural organisms as platforms for fabricating inorganic materials at ambient temperature. A significant challenge remains as to whether we can directly use biosynthetic pathways in living organisms without genetic modification, to deliberately produce anthropogenically useful materials inessential to those organisms.

The mussel is a typical bio-mineralization system for pearl formation. Among them, the fresh-water mussel *Cristaria plicata* is extensively used for culturing blister pearls of large sizes and various shapes, and is therefore a beneficial host for preparation of samples (Figure 1 a). Herein, we use *Cristaria plicata* as a cradle for synthesizing TiO_2, a material with broad applications to facilitate solving both energy and environmental problems.[14–17] To improve its energy conversion efficiency in the visible light regime, persistent efforts have been devoted to modifying its inherent band gap. In particular, nitrogen-doped TiO_2 (N-TiO_2) appears to use visible light efficiently, but heat treatments and complicated procedures are usually required during preparation.[17,18] A one-pot synthetic method for tailoring key properties of TiO_2 (such as microstructure, phase stability and light-use efficiency), especially at ambient temperature, is of great significance from an energy-saving perspective.[19]

Based on a natural pearl culture process, we demonstrate a novel "one-pot" ambient-temperature approach for fabrication of N-TiO_2 materials using living *Cristaria plicata*. Interactions between the organism and TiO_2 precursor give rise to compelling questions regarding bio-inspired synthesis, such as: the influence of the host upon chemical reactions governing formation, the structures obtainable, and the resultant properties of products. Our results show that amorphous precursor transforms into N-doped anatase TiO_2 with hierarchical nanostructure when grown inside living mussels. Synthetic TiO_2 exhibits enhanced visible-light photocatalytic activity in both chemical waste remediation and hydrogen generation.

Amorphous TiO_2 precursor was shaped into a tablet with a diameter of 10 mm and thickness of 1–2 mm, and then implanted as a pearl nucleus between the mantle and shell of *Cristaria plicata* (Supporting Information, Scheme S1). TiO_2 precursor was prepared using a typical sol–gel method, by adding 1 mL of acetic acid to 5 mL of tetrabutyl titanate. The precursor was an amorphous phase (Figure 1 b,c), even after

[*] Dr. J. J. Xie, Prof. B.-L. Su, Dr. H. Zeng, Dr. M. Wang, Prof. W. M. Wang, Prof. H. Wang, Prof. Z. Y. Fu
State Key Laboratory of Advanced Technology for Materials Synthesis and Processing
Wuhan University of Technology, Wuhan 430070 (P.R. China)
E-mail: zyfu@whut.edu.cn
Prof. H. Xie
School of Chemistry, Chemical Engineering and Life Science
Wuhan University of Technology, Wuhan 430070 (P.R. China)
Prof. B.-L. Su
Laboratory of Inorganic Materials Chemistry
University of Namur, B-5000 Namur (Belgium)
Prof. Y. B. Cheng
Department of Materials Engineering
Monash University, Victoria 3800 (Australia)
Prof. X. D. Du
Department of Pearl Research
Guangdong Ocean University, Zhanjiang 524025 (P.R. China)

Supporting information for this article, including experimental details, is available on the WWW under http://dx.doi.org/10.1002/anie.201509906.

 © 2016 Wiley-VCH Verlag GmbH & Co. KGaA, Weinheim

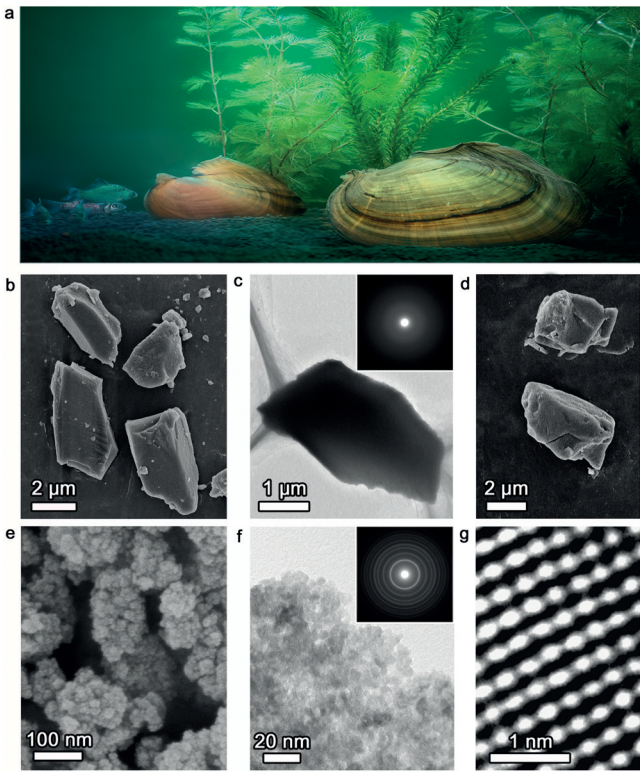

Figure 1. a) Living *Cristaria plicata*. b) SEM and c) TEM images of TiO_2 precursor. Inset: the SAED pattern. d) SEM image of TiO_2 precursor aged in air for 120 days. e) SEM image of bm-TiO_2 nanoparticles mineralized in mussel for 90 days. f) TEM image of bm-TiO_2 nanoparticles. The diffraction rings of SAED pattern are assigned to the (101), (004), (200), (211), (204), (116), and (215) planes of anatase. g) An HRTEM image of bm-TiO_2 revealing the fringes of (101) planes with a lattice spacing of about 0.33 nm.

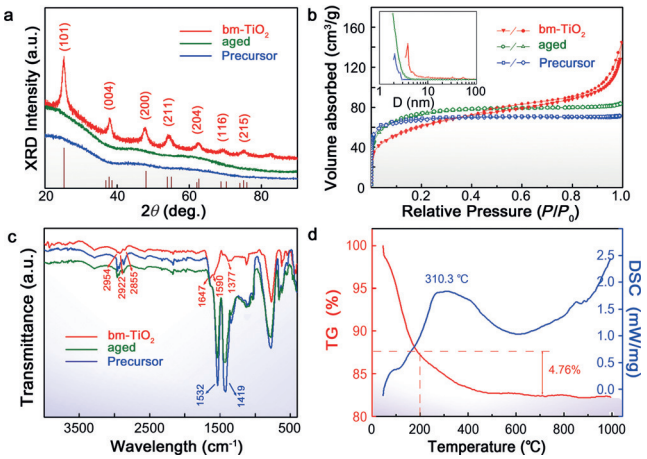

Figure 2. Structure evolution of bm-TiO_2 nanocrystals. a) X-ray diffraction analyses of TiO_2 samples. b) N_2 adsorption-desorption isotherms of TiO_2 samples. Relative pore size distributions are shown in the inset. c) FTIR spectra of TiO_2 samples. d) Thermogravimetric analysis of a bm-TiO_2 sample after mineralization.

aging in air for 120 days (Figure 1 d). However, after mineralization within the mussel's body for 90 days, agglomerates consisting of nanospherical grains were obtained (Figure 1 e). The bm-TiO_2 crystallized as shown, with well-resolved rings and lattice features in the SAED and HRTEM images (Figure 1 f,g). X-ray diffraction patterns of bm-TiO_2 present broad diffraction peaks, revealing the nanosized nature of crystallites (Figure 2 a). The crystal phase has an anatase structure with an average grain size of approximately 10 nm, in agreement with TEM observations. More detailed information about crystallization processes was obtained by a time-resolved study over the course of mineralization, starting from the earliest stage (Supporting Information, Figure S1). When the precursor was aged in air for 120 days, no sign of crystallization was observed (Supporting Information, Figure S1g). Normally, the amorphous TiO_2 obtained from the sol-gel method requires heat treatments before crystallization occurs.[19]

The BET surface area and pore volume of bm-TiO_2 were determined to be 206 $m^2 g^{-1}$ and 0.22 $m^3 g^{-1}$ respectively (Figure 2 b). The isotherm of bm-TiO_2 revealed two hysteresis loops at relative pressure range of 0.45–0.8 and 0.9–1.0, indicating the presence of hierarchical meso/macropores. The mesopore size is centered at 3.8 nm. In contrast, abundant micropores were present in the TiO_2 precursor. After aging in air for 120 days, the precursor isotherm also presented microporous features. During the biomineralization process, micropores convert into hierarchical meso/macropores due to crystallization and grain growth. Therefore, by using living mussels as platforms, hierarchically porous TiO_2 powders are synthesized at ambient temperature. Studies indicate that hierarchically porous structure can improve photocatalytic activity.[16,20]

A change in chemical composition was found in the bm-TiO_2 sample during mineralization (Figure 2 c). Precursor prepared by adding acetic acid exhibits characteristic C=O stretching vibrations at 1532 and 1419 cm^{-1}, variously coordinated to Ti as bidentate ligands,[19] which are stable and usually require post-calcination before elimination. The two bands are still visible in samples after aging in air for 120 days or after heating at 300 °C (Supporting Information, Figure S2). Interestingly, after in vivo mineralization, the bands completely disappear, implying that Ti-acetate complexes have been replaced by other species. Furthermore, several substantial bands associated with proteins are observed, corresponding to amide I, II, and III vibrational modes at 1647, 1590, and 1377 cm^{-1}, respectively.[21] To estimate the organic content, we applied a thermogravimetric analysis procedure to the fresh bm-TiO_2 (Figure 2 d). Weight loss below 200 °C is probably due to loss of water, and 4.76 % mass loss above 200 °C is induced by decomposition of organic matrices.[22]

Pristine TiO_2 was prepared as a reference by directly heating the TiO_2 precursor at 600 °C for 30 min. The results show that pristine TiO_2 has the characteristics of anatase (Supporting Information, Figure S3). A typical single O 1s peak for pristine TiO_2 is observed at 530 eV, whereas for bm-TiO_2 nanocrystals the O 1s peak is resolved into two peaks at 529.8 and 531.8 eV. The 531.8 eV peak is attributed to Ti-OH species (Supporting Information, Figure S4).[14] The broad N 1s peak in bm-TiO_2 can be deconvoluted into two peaks

© 2016 Wiley-VCH Verlag GmbH & Co. KGaA, Weinheim

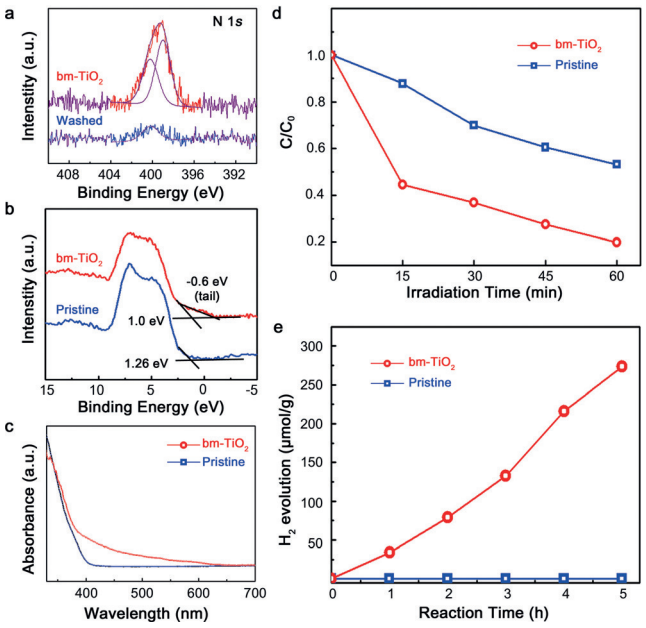

Figure 3. a) N 1s XPS spectra of bm-TiO_2 nanocrystals before and after chemical washing. The red and blue curves are XPS data, and the purple curves are the fitting of experimental data. b) Valence-band XPS spectra of TiO_2 samples. c) UV/Vis absorption spectra of TiO_2 samples. d) Visible-light-promoted photocatalytic degradation of RhB carried out by TiO_2 samples. e) Hydrogen evolved under visible light after photocatalytic water reduction using TiO_2 samples.

centered at 400.2 eV and 398.9 eV (Figure 3a). For comparison, we removed residual proteins by washing bm-TiO_2 according to a typical chemical method. After washing, the peak at 398.9 eV disappeared but the peak at 400.2 eV remained. Therefore, the peak at 398.9 eV is assigned to N–H bonds arising from residual proteins, and the peak at 400.2 eV is related to interstitial nitrogen dopant.[17,23] The atomic concentration of nitrogen was calculated based on the XPS data, revealing that 0.44 at.% N has been doped into bm-TiO_2. Pristine TiO_2 displays valence band density of states (DOS) characteristic of anatase, with a band edge about 1.26 eV below the Fermi energy. By comparison, the valance band of bm-TiO_2 shows differences: the main absorption onset is located at about 1.0 eV and the maximum energy related to the band tail blue-shifts toward the vacuum level at about 0.6 eV (Figure 3b). The band gap shift is attributed to lattice defects such as those arising from interstitial nitrogen.

Natural proteins exhibit improved mineral-forming activities in vivo, as compared to in vitro processes utilizing isolated or synthetic proteins, owing to the cellular control for these natural proteins.[24] Thus, under these special conditions, self-adding active proteins act as a nitrogen source for N-doping, which could lead to production of TiO_2 with enhanced visible-light photocatalytic activity. Pristine TiO_2 is unable to absorb visible radiation owing to its relatively large band gap[17] (Figure 3c), whereas bm-TiO_2 shows visible light absorption from 380–650 nm owing to interstitial nitrogen doping. bm-TiO_2 exhibits superior photocatalytic activity in degradation of Rhodamine B (RhB) compared with pristine TiO_2 (Figure 3d). The photocatalytic activity of bm-TiO_2 does not significantly decrease even after five cycles of photodegradation, implying that these photocatalysts are very stable (Supporting Information, Figure S5a). Notably, pristine TiO_2 also demonstrates photocatalytic activity under visible light owing to a self-sensitized degradation process.[25] To eliminate this effect, phenol degradation was also investigated and a similar superior performance was observed in the presence of bm-TiO_2 nanocrystals (Supporting Information, Figure S5b).

A photocatalytic test for hydrogen evolution was carried out under visible light (Figure 3e). No obvious hydrogen production was observed using pristine TiO_2, as expected. Whereas for bm-TiO_2 the average rate of hydrogen production increased to 55 μmol $h^{-1}g^{-1}$, reflecting the activity of nitrogen interstitial gap states.[14,17] A limited number of reports demonstrate that TiO_2 material fabricated at ambient temperature has the ability to produce hydrogen under visible-light irradiation. Thus, it can be concluded that the visible-light efficiency of TiO_2 is improved directly in *Cristaria plicata* at ambient temperature.

Stability of the anatase phase is also an important factor for TiO_2 photocatalysts. Previous studies indicate that anatase to rutile phase transformation usually occurs at 500–700 °C.[19] In the present work, TiO_2 precursor completely transforms into rutile at 700 °C. In contrast, the temperature required for phase conversion of bm-TiO_2 increases to 1000 °C (Supporting Information, Figure S6), revealing the high phase-stability of this material.

In the present work, hierarchically meso/macroporous *N*-TiO_2 is obtained in living *Cristaria plicata* at ambient temperature with excellent properties. Our findings inspire a new synthesis technique to fabricate materials by directly using natural organisms. To support and extend the current research, we also investigated the mineralization of other materials in mussels and obtained numerous interesting results. For example, macroscopic $CaCO_3/Fe_2O_3$ composite rods were formed by oriented growth of single-crystal $CaCO_3$ along implanted Fe_2O_3 nanocrystals (Supporting Information, Figure S7a). Oriented MgO material with enhanced absorptive activity was obtained via self-organization and mesoscale transformation (Supporting Information, Figure S7b).

To understand how living organisms direct the formation of these materials, proteins in a bm-TiO_2 sample were extracted and analyzed by mass spectrometry. Extracellular matrices were deemed to be involved in the bio-mineralization processes for nacre.[12,13] However, almost all the identified proteins are intracellular proteins. Actin and histone are the most abundant among these, constituting the cytoskeleton and chromatin, respectively (Supporting Information, Table S1; Figure 4). Most identified segments of actin are on the surface and are therefore accessible to TiO_2 (Figure 4; Supporting Information, Figure S8). Ubiquitin, a cytoplasmic protein that regulates the inflammatory responses and programmed cell death, was also identified; thereby implying that cell lysis occurs during mineralization of TiO_2. As reported,[26–28] nanomaterials such as TiO_2 could induce various kinds of cytotoxicity, which cause a stress responses in mussels other than death. Amorphous TiO_2 exhibits enhanced cytotoxicity in comparison with the anatase

 © 2016 Wiley-VCH Verlag GmbH & Co. KGaA, Weinheim

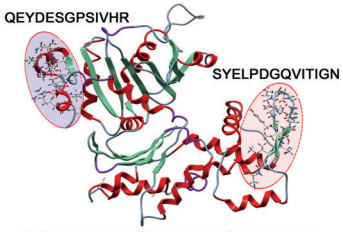

Actin structure with two identified peptides

Representative proteins identified by mass spectroscopy

Identified Proteins	Subcellular Location
Actin	Cytoplasm
Histones H_4, H_2A, H_2B	Nucleus
Ubiquitin	Cytoplasm
Glyceraldehyde 3-phosphate dehydrogenase	Cytoplasm
Cu-Zn superoxide dismutase	Cytoplasm

Figure 4. Representatives of the proteins or peptides found in bm-TiO_2 nanocrystals.

phase.[28] Pearl production is usually initiated by implanting an inorganic bead (pearl nucleus). The bead is gradually encapsulated by vast cells such as hemocytes.[13] In the present case, cytotoxicity of the amorphous TiO_2 precursor acting as a bead may lead to cell rupture. Intracellular proteins released into the bead direct the amorphous-to-anatase transition, thereby lowering the cytotoxicity of TiO_2 toward mussels.[27,28] In a sense, this phase transition may be physiologically required by the mussel. Additionally, some proteins may further degrade and produce ammonia, phenols and amines in living system, which may also promote nitrogen doping at ambient temperature.[29]

It is known that the amorphous-to-anatase phase transition is accomplished by structural rearrangement of TiO_6^{2-} octahedral units. The dehydration between octahedra, resulting in shared edges, is the rate-limiting step of this transition.[30] It is possible that in vivo crystallization of TiO_2 relies on biomolecules to control phase transition by removing H_2O, which also occurs in $CaCO_3$ biomineralization.[11] Taking peptides from actin as an example (Supporting Information, Figure S9), we hypothesize that the OH groups of proteins may act as a proton transfer catalyst[31] to facilitate the dehydration. A density functional theory (DFT) study was also performed (Supporting Information, Figure S10).[32–34] It was found that direct dehydration has an energy barrier of 18.5 kcal mol^{-1}. In contrast, OH-catalyzed dehydration adopts a proton-transport catalysis strategy with a low energy barrier of 10.9 kcal mol^{-1}.

We also set up in vitro experiments in three kinds of aqueous solutions (Supporting Information, Figure S11): with actin, water, and extrapallial fluid protein. HRTEM and SEAD clearly indicate that an acceleration of the crystallization process is achieved in actin solution. XRD patterns also show that the crystallization process is faster in actin. However, no nitrogen doping occurs during in vitro mineralization, suggesting that doping is induced by the synergistic effects present in living systems (Supporting Information, Figure S12). Therefore, the detailed mechanism of in vivo formation is not easily accessible by in vitro experiments. Additional work with further controls on the mineralization process will be carried out in the future.

In conclusion, for the first time, living mussel has been used as a cradle for fabrication of TiO_2 materials (which are not required in its physiological processes) with optimized properties at ambient temperature. Although this technique is still in its infancy, our approach extends present chemical methodologies for material production, especially under environmentally benign conditions.

Acknowledgements

We thank S. H. Xie (Guangdong Pear Company) for kindly providing living mussels and supporting fields for experiments; J. G. Yu and Y. Li (Wuhan University of Technology) for their help on the photocatalytic experiments. Financial support from National Natural Science Foundation of China (51521001, 21103130, and 61274135) and the Ministry of Science and Technology of China (2015DFR50650) are acknowledged. All calculations were performed on the cluster of the Key Laboratory of Theoretical and Computational Photochemistry, Ministry of Education.

Keywords: ambient temperature · bioprocess-inspired synthesis · intracellular proteins · natural organisms · nitrogen-doped TiO_2

How to cite: *Angew. Chem. Int. Ed.* **2016**, *55*, 3031–3035
Angew. Chem. **2016**, *128*, 3083–3087

[1] S. Weiner, W. Traub, H. D. Wagner, *J. Struct. Biol.* **1999**, *126*, 241.
[2] J. Aizenberg, A. Tkachenko, S. Weiner, L. Addadi, G. Hendler, *Nature* **2001**, *412*, 819.
[3] A. Veis, *Science* **2005**, *307*, 1419.
[4] E. Munch, M. E. Launey, D. H. Alsem, E. Saiz, A. P. Tomsia, R. O. Ritchie, *Science* **2008**, *322*, 1516.
[5] L. Jiang, Y. Zhao, J. Zhai, *Angew. Chem. Int. Ed.* **2004**, *43*, 4338; *Angew. Chem.* **2004**, *116*, 4438.
[6] W. L. Noorduin, A. Grinthal, L. Mahadevan, J. Aizenberg, *Science* **2013**, *340*, 832.
[7] S. Mann, *Biomineralization*, Oxford University Press, Oxford, **2001**.
[8] W. D. Kingery, *Introduction to ceramics*, Wiley, New York, **1960**.
[9] S. L. Sewell, D. W. Wright, *Chem. Mater.* **2006**, *18*, 3108.
[10] C. Du, G. Falini, S. Fermani, C. Abbort, J. Moradian-Oldak, *Science* **2005**, *307*, 1450.
[11] N. Kŕoger, M. B. Dickerson, G. Ahmad, Y. Cai, M. S. Haluska, K. H. Sandhage, N. Poulsen, V. C. Sheppard, *Angew. Chem. Int. Ed.* **2006**, *45*, 7239; *Angew. Chem.* **2006**, *118*, 7397.
[12] L. Addadi, D. Joester, F. Nudelman, S. Weiner, *Chem. Eur. J.* **2006**, *12*, 980.
[13] M. Awaji, A. Machii, *Aqua-Bio Science Monographs* **2011**, *4*, 1.
[14] X. B. Chen, L. Liu, P. Y. Yu, S. S. Mao, *Science* **2011**, *331*, 746.
[15] G. Q. Zhang, H. B. Wu, T. Song, U. Paik, X. W. Lou, *Angew. Chem. Int. Ed.* **2014**, *53*, 12590; *Angew. Chem.* **2014**, *126*, 12798.
[16] J. G. Yu, Y. R. Su, B. Cheng, *Adv. Funct. Mater.* **2007**, *17*, 1984.
[17] J. Wang, D. N. Tafen, J. P. Lewis, Z. L. Hong, A. Manivannan, M. J. Zhi, M. Li, N. Q. Wu, *J. Am. Chem. Soc.* **2009**, *131*, 12290.
[18] R. Asahi, T. Morikawa, T. Ohwaki, K. Aoki, Y. Taga, *Science* **2001**, *293*, 269.

 © 2016 Wiley-VCH Verlag GmbH & Co. KGaA, Weinheim

[19] J. F. Ye, W. Liu, J. G. Cai, S. Chen, X. W. Zhao, H. H. Zhou, L. M. Qi, *J. Am. Chem. Soc.* **2011**, *133*, 933.
[20] Y. Li, Z. Y. Fu, B. L. Su, *Adv. Funct. Mater.* **2012**, *22*, 4634.
[21] P. R. Carey, *Biochemical Applications of Raman and Resonance Raman Spectroscopies*, Academic Press, New York, **1982**, chap. 4.
[22] Y. J. Lee, H. Yi, W.-J. Kim, K. Kang, D. S. Yun, M. S. Strano, G. Ceder, A. M. Belcher, *Science* **2009**, *324*, 1051.
[23] V. Etacheri, M. K. Seery, S. J. Hinder, S. C. Pillai, *Chem. Mater.* **2010**, *22*, 3843.
[24] L. B. Gower, *Chem. Rev.* **2008**, *108*, 4551.
[25] W. Zhao, C. C. Chen, W. H. Ma, J. C. Zhao, D. X. Wang, H. Hidaka, N. Serpone, *Chem. Eur. J.* **2003**, *9*, 3292.
[26] M. I. Setyawati, C. Y. Tay, *Nat. Commun.* **2013**, *4*, 1673.
[27] Z. Xu, X. W. Liu, Y. S. Ma, H. W. Gao, *Environ. Sci. Pollut. Res.* **2010**, *17*, 798.
[28] I. L. Hsiao, Y. J. Huang, *Sci. Total Environ.* **2011**, *409*, 1219.
[29] C. Burda, Y. L. Lou, X. B. Chen, A. C. S. Samia, J. Stout, J. L. Gole, *Nano Lett.* **2003**, *3*, 1049.
[30] Y. Kazumichi, O. James, *J. Phys. Chem. B* **1999**, *103*, 7781.
[31] Q. F. Shi, X. Li, Y. Z. Xia, L. M. Zhang, Z. X. Yu, *J. Am. Chem. Soc.* **2007**, *129*, 15503.
[32] C. Lee, T. W. T. Yang, R. G. Parr, *Phys. Rev. B* **1988**, *37*, 785.
[33] M. J. Frisch, Gaussian 09, revision A.02; Gaussian, Inc.: Wallingford, CT, **2009**, 785.
[34] K. Fukui, *Acc. Chem. Res.* **1981**, *14*, 363.

Received: October 23, 2015
Revised: November 30, 2015
Published online: January 28, 2016

 © 2016 Wiley-VCH Verlag GmbH & Co. KGaA, Weinheim